Accurate Analysis of Multi-Mode Interferometric Optical Fiber Sensor

Lijun LI[1], Congying JIA[1], Qian MA[1,2*], and Tianzong XU[1]

[1]*College of Electronic and Information Engineering, Shandong University of Science and Technology, Qingdao 266590, China*

[2]*State Key Laboratory of Mining Disaster Prevention and Control Co-Founded by Shandong Province and the Ministry of Science and Technology, Qingdao 266590, China*

[*]Corresponding author: Qian MA E-mail: qianma@sdust.edu.cn

Abstract: In view of the problem that the sensing characteristics of the multi-mode interferometric fiber sensors cannot be accurately analyzed, an analysis method based on the fast Fourier transform (FFT) and inverse fast Fourier transform (IFFT) is proposed and demonstrated theoretically and experimentally. The suitabilities of the rectangular window function with the narrow main lobe (high spectrum resolution) and low side lobe (high main mode energy leakage) and the Hanning window function with the wide main lobe (low spectrum resolution) and high side lobe (high energy concentration) in this kind of sensor analysis are discussed, respectively. This method can not only realize the sensing performance analysis of the various modes, but also overcome the inconsistency of the different interference wavelength (dip) sensing characteristics in the conventional analysis methods. At the same time, this method is also beneficial to solve the repetitive problem of such sensors.

Keywords: Window function; FFT; optical fiber interferometric sensor; analysis method

Citation: Lijun LI, Congying JIA, Qian MA, and Tianzong XU, "Accurate Analysis of Multi-Mode Interferometric Optical Fiber Sensor," *Photonic Sensors*, 2024, 14(1): 240124.

1. Introduction

All in-fiber interferometers are a type of multi-mode interferometric fiber sensor appeared in recent years, such as the Mach-Zehnder (M-Z) interferometer [1, 2], Michelson interferometer [3, 4], and micro nano fiber [5, 6] based on the core mode and multi cladding modes interference working principle. Due to the large number of cladding modes and the relatively large mode field diameter, this kind of sensor presents good sensing characteristics in the detection of the surrounding material refractive index (RI) (solids, liquids, and gases) [7–9], stress [10, 11], temperature [12, 13], electromagnetic field [14, 15], etc. In addition, these sensors also have the advantages of the simple structure, low cost, and anti-electromagnetic interference. At present, the analysis method to measure the peaks or dips wavelengths of the interference spectrum changing with the measured quantity is conventionally adopted. In 2015 [16], a liquid level sensor based on an in-fiber M-Z interferometer experimentally was demonstrated, and two different dips were investigated, which showed the 0.0174 nm/mm sensitivity with the 97.4% linearity at the 1560 nm wavelength, and the

Received: 13 April 2023 / Revised: 25 September 2023

DOI: 10.1007/s13320-023-0701-1
Article type: Regular

0.102 5 nm/mm sensitivity with the 99.23% linearity at the 1 570 nm wavelength, respectively. In 2019, Jiao *et al*. [17] proposed an M-Z interferometer based on the single mode-multimode-thinned core-single mode optical fiber structure for RI sensing, and in their experiments, two dips were monitored, which had the −18.176 4 nm/RIU sensitivity and 98% linearity at the 1 580 nm wavelength, and the −12.219 7 nm/RIU sensitivity and 97% linearity at the 1 592 nm wavelength, respectively. In 2021, Wang *et al*. [18] proposed an M-Z interferometric optical fiber strain sensor, in which two dips presented the 165 pm/με sensitivity and 99.6% linearity at the 1 546 nm wavelength, and the 145.25 pm/με sensitivity and 99.6% linearity at the 1 629 nm wavelength, respectively. In 2018 [19], the sensing characteristics of a seawater temperature sensor based on the M-Z interferometer was studied through investigating its interference peaks at different wavelengths with the 40.26 pm/℃ sensitivity and 99.8% linearity at the dip of 1 245 nm and the 38.24 pm/℃ sensitivity and 99.5% linearity at the dip of 1 547 nm, respectively. According to the relevant literature, it can be found that different wavelengths of the sensor exhibit different sensitivities and linearities because different interference wavelengths (dips or peaks) contain different compositions of cladding modes [10, 11, 17]. The principle of multi-mode interference makes the sensing process of this kind of sensor very complex. However, the current analysis method of the sensing characteristics of such sensors is very rough, and the methods analyzed solely from the wavelength drift rather than the working mode may lead to detailed sensing principles and sensing processes being ignored [16–19]. Therefore, an accurate analysis method for sensing performance of the multi-mode interferometric sensor is urgently needed.

In this paper, a novel fast Fourier transform (FFT) based analytical method is proposed, and it is applied to the analysis of a liquid RI sensing properties of a fiber optical M-Z interferometric sensor. In this process, the FFTs with the rectangular and Hanning window functions are analyzed, respectively. By using the FFT of the interference spectrum of the sensing process, the spatial spectrum of the sensing mode can be distinguished. By using the inverse fast Fourier transform (IFFT) for the spatial spectrum of the sensing mode, the interference spectrum of the mode can be obtained. The results show that the FFT through the rectangular window function can obtain a high-resolution spatial spectrum, which is suitable for the investigation of the sensing modes and the sensing performance analysis of a sensor with a small number working modes, and the FFT through the Hanning window function can obtain a spatial spectrum with an energy concentration sensing mode, which is suitable for the investigation of the sensing mode and the sensing performance analysis of a sensor with more working modes. By using this novel analysis method, the interference spectra, corresponding to the same mode, show uniform sensing properties, such as the same wavelength drift direction, sensitivity, and linearity. Therefore, this Fourier transform method can solve the problem that the sensing characteristics cannot be accurately analyzed, and it can also solve the problems of the poor repeatability and demodulation difficulties of the multi-mode interferometric optical fiber sensor.

2. Theoretical analysis

Any continuously measured signal can be expressed as an infinite superposition of sine wave signals at different frequencies using the discrete Fourier transform (DFT) [20]. In addition, the FFT is a highly efficient algorithm for the DFT. The spectrum output of the interference sensor acts as a time-stationary signal, and the relevant modes of spatial frequency information can be obtained by applying the FFT. In this process, the window function selection is important. As known, the main lobe and side lobe of the window function directly

affect the FFT spectrum processing results, the specific performance of the main lobe width mainly determines the spectrum resolution of the signal, and the side lobe is related to the energy distribution [21]. Generally speaking, the higher the side lobe is, the more serious the energy leakage undergoing the FFT is, and the smaller the side lobe energy is. The signal energy is relatively concentrated in the main lobe, which reflects the more accurate spectrum information of the original signal [22]. Therefore, two representative window functions of the rectangular window and Hanning window are selected.

Assuming the time range is $0 \le t \le T$, the time domain expression of the rectangular window function can be expressed as

$$W(t) = 1. \tag{1}$$

And the time domain expression of the Hanning window function can be expressed as

$$W(t) = \frac{1}{2}\left(1 - \cos\frac{2\pi t}{T}\right). \tag{2}$$

The time domain and frequency domain spectra of the two window functions are shown in Figs. 1(a)–1(d), respectively. Comparing Figs. 1(b) and 1(d), it can be found that the rectangular window function has a narrow main lobe and a high side lobe. It means that the single after the FFT using rectangular windows will have the high frequency resolution and be easy to generate the high-frequency leakage. In comparison, the Hanning window has a relatively wide main lobe and a relatively low side lobe. It means that the frequency resolution is reduced and the spectral energy leakage is decreased.

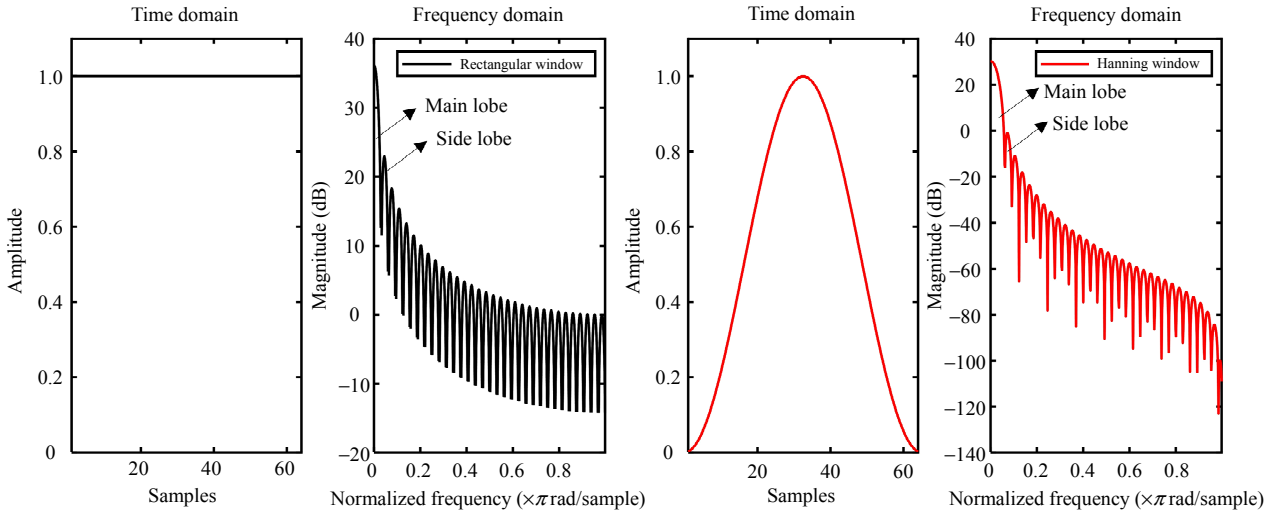

(a) (b) (c) (d)

Fig. 1 Time domain and frequency domain spectra of different functions: (a) time domain and (b) frequency domain spectra of the rectangular window function, respectively; (c) time domain and (d) frequency domain spectra of the Hanning window function, respectively.

An all-fiber M-Z interferometer is analyzed based on a single mode-thinned core-single mode optical fiber (STS) structure. The incident light propagating through the lead-in single-mode fiber (SMF) is split into two parts at the first splicing point. One part transmits in the fiber core while the other enters the cladding of the thin-core fiber (TCF), resulting in exciting the cladding modes by the core mismatch. The two beams of the light couple at the second splicing point between the TCF and the output SMF, which forms an M-Z interference. According to [23], the effective RI difference based on the all-fiber interferometer can be obtained by the spatial frequency:

$$\xi = \frac{1}{\lambda_0^2}\Delta m_{\text{eff}} L \tag{3}$$

where ξ is the spatial frequency, λ_0 is the central wavelength, L is the length of the sensing fiber, and Δm_{eff} is the effective RI difference between the core mode and the cladding mode. In order to get the effective RI difference, the simulation output spectrum, shown in Fig. 2(a), is chosen to do the FFT with the rectangular and Hanning window functions, respectively. Figure 2(b) shows its spatial spectrum by using the FFT with two different window functions, respectively. By solving the effective RI of the cladding mode of the sensing fiber with the interval traversal and chord cutting method, the order of the mode corresponding to the cladding mode can be determined, which is shown in Fig. 2(c), so that the order of the cladding mode corresponding to the peak values in the spatial spectrum can be obtained. From Fig. 2, it can be found that there are the core mode and cladding modes in the spatial frequency spectrum by using the rectangular windows transformation, the cladding modes can be finely separated, but the energy is relatively low and leaks to the higher order weakly modes, and in the spatial frequency spectrum of the Hanning window transformation, the cladding mode is presented as one mode group with the relatively concentrated energy.

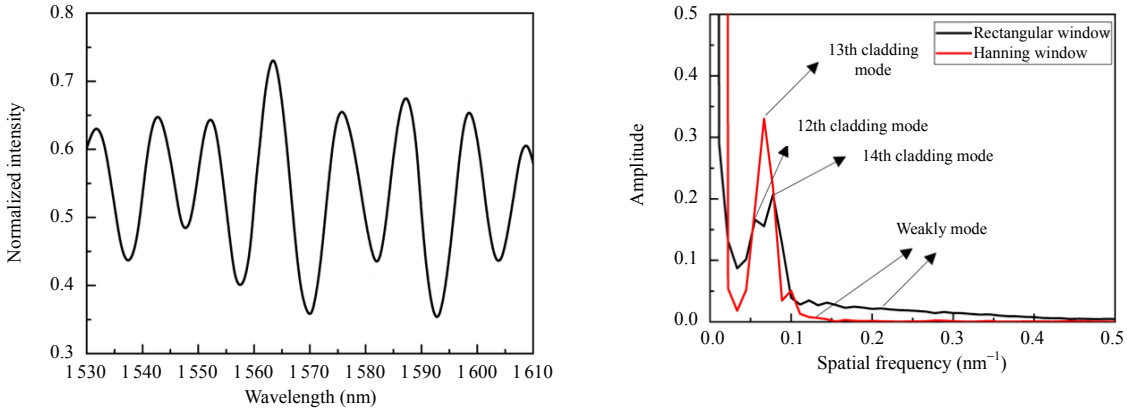

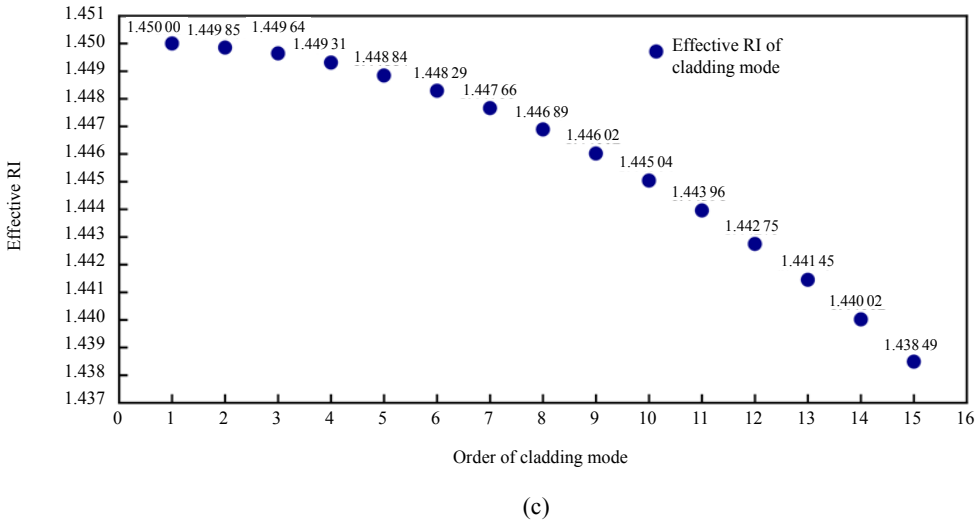

Fig. 2 Simulation spectra of the all-fiber M-Z interferometric sensor: (a) simulation output spectrum and its (b) spatial frequency spectrum by using the FFT with the rectangular and Hanning window functions, respectively, and (c) scatter plot of the effective RI and the cladding mode order of the MZI.

3. Experiments

3.1 Analysis of an interferometric optical fiber RI sensor by the conventional method

A refractometer with the all-fiber structure that the 30-mm-long TCF (4.5 μm/125 μm core/cladding) spliced between two standard SMFs (8.3 μm/125 μm core/cladding) is fabricated and experimentally investigated. The setup is shown in Fig. 3, and a broad band source (BBS) and an optical spectrum analyzer (OSA, Yokogawa AQ 6370 with the 0.05 nm resolution) are adopted to observe the interferometric spectrum of the sensor. The two ends of the sensor are fixed on the glass slide with a microgroove used to immerse in the tested liquid in the RI range of 1.3364–1.4200, respectively. The sensor is washed with the deionized water several times in order to clean the surface of the sensor after every RI value measurement.

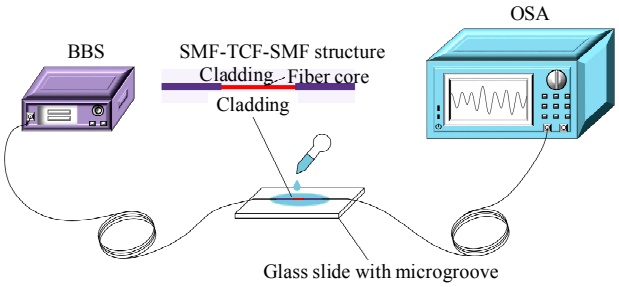

Fig. 3 Schematic diagram of the experimental setup.

To understand the sensing characteristics of the sensor with different numbers of cladding modes, two liquids with different RI ranges of 1.3364–1.3554 and 1.3724–1.4200 are adopted. The superposition diagrams of the interference spectra of the sensor at different liquid RI ranges are shown in Figs. 4(a) and 4(b), respectively. From

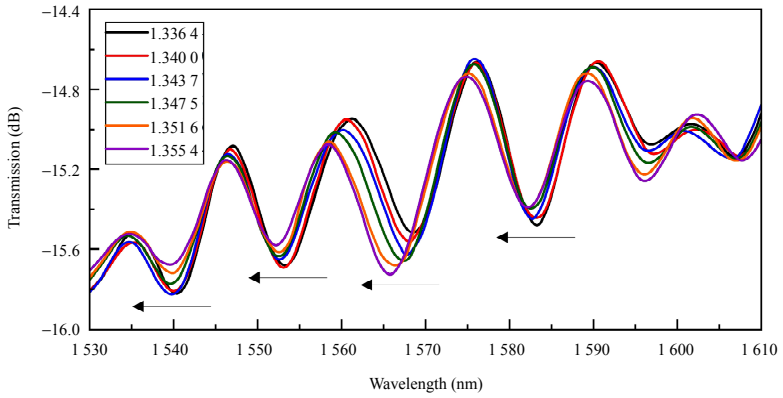

(a)

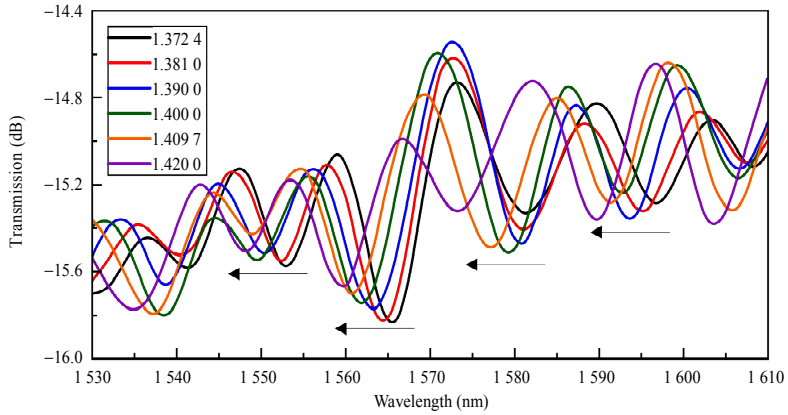

(b)

Fig. 4 Superposition diagram of the interference spectrum of the sensor: liquid RI range from (a) 1.3364 to 1.3554 and (b) 1.3724 to 1.4200, respectively.

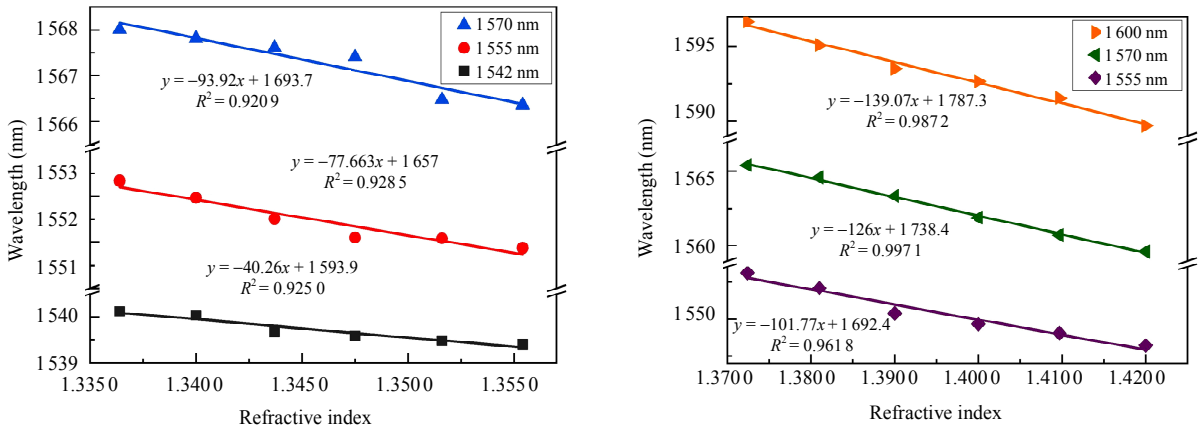

Fig. 5 Linear fitting diagrams of different dips drifts with the RI change from (a) 1.336 4 to 1.355 4 and (b)1.372 4 to 1.420 0, respectively.

these figures, it can be found that all the interference intensity dips are blue shifts with the RI increase. The linear fittings of different dips drifts with the RI changing from 1.336 4 to 1.355 4 are shown in Fig. 5(a). From Fig. 5(a), it can be found that different dips correspond to different sensitivities and linearities as reported literature [17, 24, 25] and as in our experiments, such as the –40.66 nm/RIU sensitivity and 92.5% linearity at the dip of 1 542 nm, the –77.66 nm/RIU sensitivity and 92.85% linearity at the dip of 1 555 nm, and the –93.92 nm/RIU sensitivity and 92.09% linearity at the dip of 1 570 nm. The linear fittings of different dips drift with the RI changing from 1.372 4 to 1.420 0 are shown in Fig. 5(b). From Fig. 5(b), it also can be found that different interference wavelengths correspond to different sensitivities and linearities with higher values because more high-order cladding modes are excited as the RI of the surrounding medium increases, such as the –101.77 nm/RIU sensitivity and 96.18% linearity at the dip of 1 555 nm, the –126 nm/RIU sensitivity and 99.71% linearity at the dip of 1 570 nm, and the –139.07 nm/RIU sensitivity and 98.72% linearity at the dip of 1 600 nm. This is mainly because different interference wavelengths (dips or peaks) contain many different modes, meanwhile, different modes have different sensing properties, resulting in different interference wavelengths corresponding to different sensitivities. Thus, we can see that the conventional sensing characteristics analysis method can lead to the problem that the sensing characteristics of this kind of sensor cannot be determined.

3.2 Accurately analysis of the sensor by the FFT analysis method

In order to accurately analyze the sensing characteristics of the sensor, the sensing modes must be clearly defined. Therefore, the output interference spectrum is transformed by the FFT under the rectangular window and Hanning window functions, respectively.

Firstly, the rectangular window is adopted for the interferent spectrum of the sensor to obtain the sensing modes of the sensor responding to 1.336 4–1.355 4 and 1.372 4–1.420 0 liquid RI ranges, from which the spatial frequency composition by using the FFT of the sensing performance with the RI change is shown in Figs. 6(a) and 6(b), respectively. From Figs. 6(a) and 6(b), it can be found that several cladding modes involved in the sensing are obtained. From Fig. 6(a), it can be found that there are three main modes, which are the 9th, 12th, and 14th modes, respectively. From Fig. 6(b), five main modes of the 9th, 11th, 12th, 13th, 14th modes are observed. From its detail changing in the sensing process in Fig. 6(b), it can be found that the cladding modes fluctuate disordered during sensing,

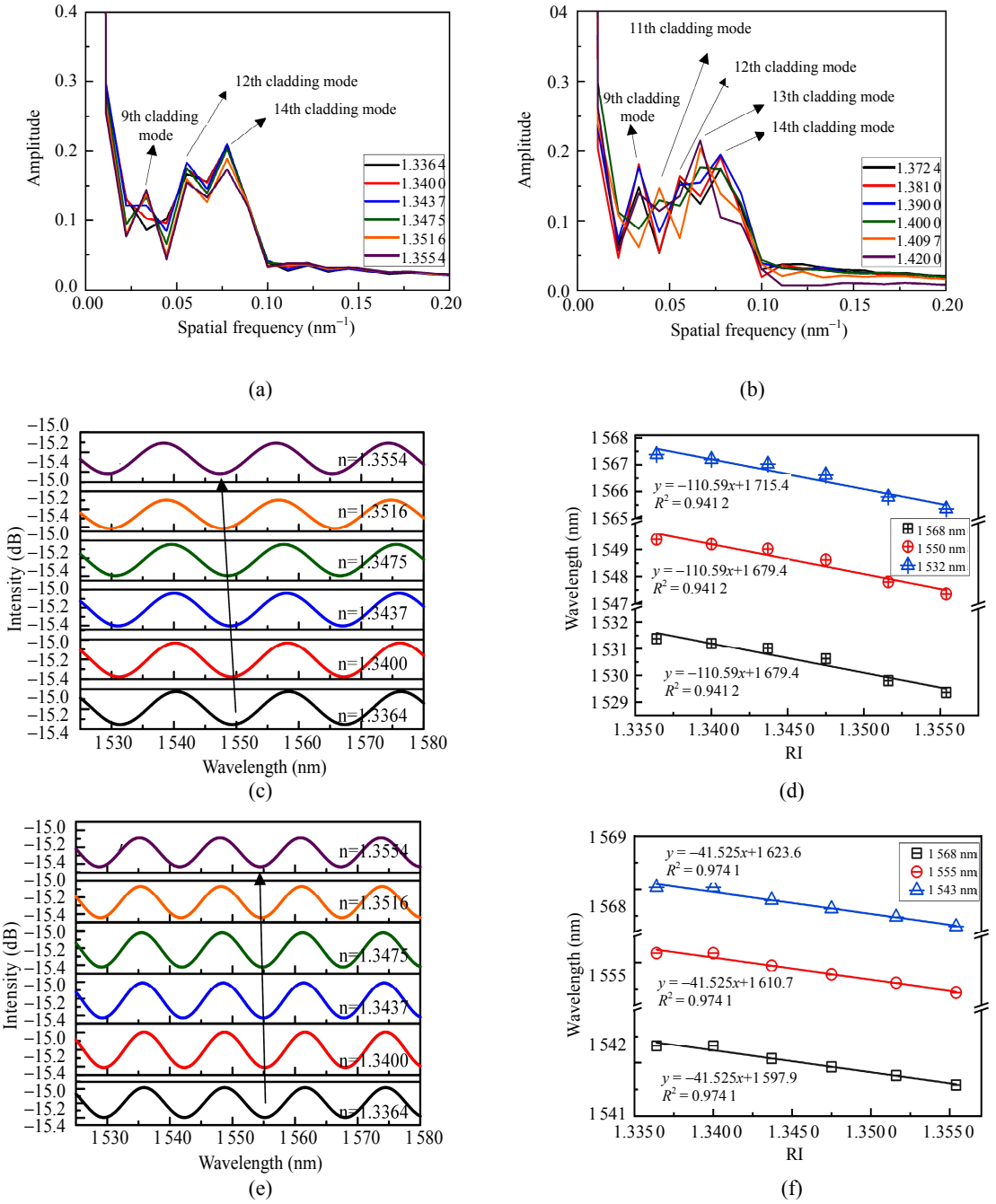

Fig. 6 Spatial frequency composition of the sensor through the FFT with the RI range: (a) 1.3364–1.3554 and (b) 1.3724–1.4200, respectively; (c) interference spectrum after the IFFT and (d) sensing characteristics curve diagram of the 12th order mode, respectively; (e) Interference spectrum after the IFFT and (f) the sensing characteristics curve diagram of the 14th order mode, respectively.

due to that the rectangular window is a kind of high resolution narrow main lobe and high frequency leakage low side lobe in the FFT. Therefore, it can be seen that the rectangular window is not suitable to be applied to the sensing performance analysis of such sensors in the high RI range (sensors with more working modes). From Fig. 6(a), the detailed analysis of the mode-sensing process reveals that the 9th order cladding mode is unstable due to the reason that

when the external RI environment is low, only some low-order cladding modes in the sensing structure are excited and interfere with the core mode. The higher-order cladding modes are excited and hopped as the external RI increases. The detail changes of the 12th and 14th cladding modes in the sensing process are shown in Fig. 6(a). By using the IFFT, the interference spectra of the 12th and 14th order modes are shown in Figs. 6(c) and 6(d), respectively. By tracking the dip wavelength drift with the liquid RI change, the sensing characteristics curve diagram of 12th and 14th order modes can be obtained, which are shown in Figs. 6(e) and 6(f), respectively. From these figures, the sensing sensitivity corresponding to the 12th cladding mode is –110.59 nm/RIU with the 94.12% linearity, and the sensing sensitivity corresponding to the 14th cladding mode is –41.525 nm/RIU with the 97.41% linearity, respectively. By this new method, it can be found that it can be found that all the dips corresponding to the same working mode present a uniform sensing characteristic.

Secondly, the Hanning window is adopted for the interference spectrum of the sensor by the FFT. The Hanning window has a wider main lobe and a higher side lobe than those of the rectangular window, which makes the modes energy in the spatial spectrum more concentrated. The spatial spectrum of the sensing process in the RI range of 1.3364–1.3554 by applying the FFT to the optical spectrum of the sensor is shown in Fig. 7(a), and it shows the IFFT of the spatial spectrum of the sensing, from which it can be seen that there is only one main mode (the 13th order cladding mode). After process, its interference spectrum is obtained, as shown in Fig. 7(c), from which it can be seen that all the dips are blue shifts with the RI increase, and its linear fitting curves of some dips are shown in Fig. 7(b). From Fig. 7(b), all the dips

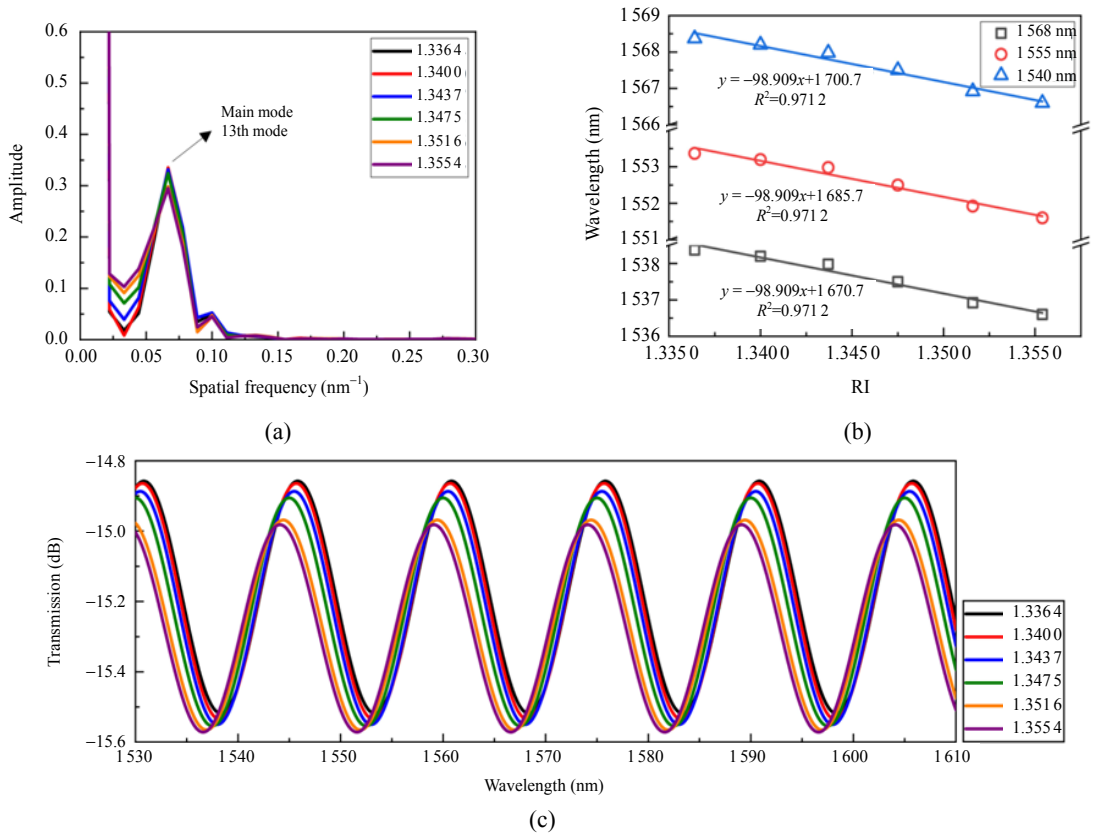

Fig. 7 Hanning window processing results with the RI range of 1.3364–1.3554: (a) spatial spectrum, (b) superimposed interference spectra after the IFFT, and (c) linear fitting curves of some dips.

present the uniform sensitivity of –98.909 nm/RIU and linearity of 97.12%. Similarly, the Hanning window is applied to the sensing performance analysis in the RI range of 1.3724–1.4200. The obtained spatial spectrum is shown in Fig. 8(a). In this figure, there is a relatively broad main mode that has been relatively stable throughout the RI change. By using the IFFT, the superimposed interference spectra are shown in Fig. 8(c). As seen in Fig. 8(c), all the dips present blue shifts with the RI increase. The linear fitting curves of some dips are shown in Fig. 8(b). As shown, the sensor exhibits a uniform sensitivity of –141.65 nm/RIU and linearity of 98.83%.

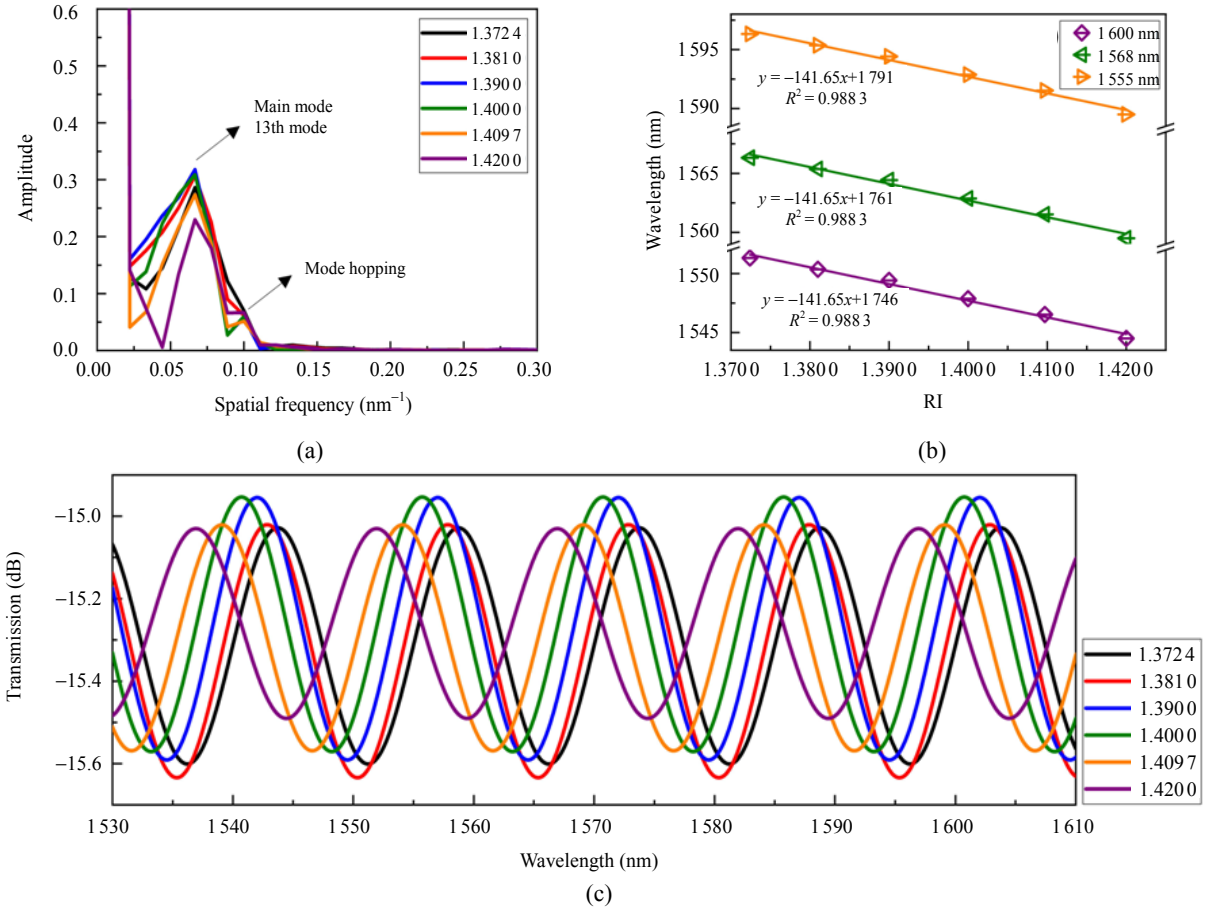

Fig. 8 Hanning window processing results with the RI range of 1.3724–1.4200: (a) spatial spectrum, (b) superimposed interference spectra by using the IFFT, and (c) linear fitting curves of some dips.

4. Conclusions

In conclusion, a novel accurate sensing characteristics analysis method based on the Fourier transform applied to the optical spectrum of the multi-mode field interferometric optical fiber sensor is proposed and demonstrated. With the rectangular window and the Hanning window functions, the sensing characteristics of the optical fiber interferometric sensor in the case of the narrow main lobe and low side lobe window functions, and wide main lobe and high side lobe window functions in the low and high RI ranges are analyzed, respectively. Compared with the conventional methods, this method can not only clearly observe the change of the mode in the sensing process, but also obtain the sensing characteristics of each sensing mode, so as to effectively overcome the difficulty of the sensing characteristics analysis by using the conventional analysis methods. In our experiment, in the low RI range, relatively few cladding modes are excited in the sensor, so with the

high-resolution window function, and the sensing characteristics of different modes in detail can be observed and analyzed. In the high RI range, more high-order cladding modes are excited, and the high-resolution window function is no longer applicable. Then, by using the Fourier transform analysis method with the window function, when the energy concentration wide main lobe and high side lobe are adopted, the problem of many high-order cladding modes analysis can be solved. Therefore, this method based on the Fourier transform can solve the problem that the sensing characteristics of the sensors cannot be accurately analyzed, and it can also solve the problems of poor repeatability and demodulation difficulties. The proposed method is of great significance to promote the development of sensors to the practical application.

Acknowledgment

This work was supported by the State Key Laboratory of Mining Disaster Prevention and Control, Shandong University of Science and Technology (Grant Nos. MDPC201602 and MDPC2022ZR04); Department of Education of Shandong Province (Grant No. J06P14); The Qingdao Feibo Technology Co., Ltd. (Grant No. 02040102401); Postdoctoral Research Foundation of China (Grant Nos. 200902574 and 20080441150).

Declarations

Conflict of Interest The authors declare that they have no competing interests.

References

[1] P. C. Chen, X. W. Shu, and K. Sugden, "Compact assembly-free vector bend sensor based on all-in-fiber-core Mach-Zehnder interferometer," *Optics Letters*, 2018, 43(3): 531–534.

[2] F. Mumtaz, Y. T. Dai, and M. A. Ashraf, "Inter-cross demodulated refractive index and temperature sensor by an etched multicore fiber of a MZI structure," *Journal of Lightwave Technology*, 2020, 38(24): 6948-6953.

[3] N. M. Kerschbaumer, L. I. Fochler, M Reichenspurner, S Rieger, M Fedoruk, J Feldmann, *et al.*, "Twisted light Michelson interferometer for high precision refractive index measurements," *Optics Express*, 2022, 30(16): 29722–29734.

[4] Z. Y. Xiong, C. Y. Guan, Z. Y. Duan, T. L. Cheng, P. Ye, J. Yang, *et al.*, "All-optical vector magnetic field sensor based on a side-polished two-core fiber Michelson interferometer," *Optics Express*, 2022, 30(13): 22746–22754.

[5] Y. X. Zhang, X. X. Wang, X. Y. Tang, Z. H. Liu, Y. Zhang, C. Y. Sha, *et al.*, "Photosensitive polymer-based micro-nano long-period fiber grating for refractive index sensing," *Journal of Lightwave Technology*, 2021, 39(21): 6952–6957.

[6] X. G. Li, N. Chen, X. Zhou, Y. N. Zhang, Y. Zhao, L. V. Nguyen, *et al.*, "In-situ DNA detection with an interferometric-type optical sensor based on tapered exposed core microstructured optical fiber," *Sensors and Actuators B: Chemical*, 2022, 351: 130942.

[7] X. Y. Sun, X. R. Dong, Y. W. Hu, H. T. Li, D. K. Chu, J. Y. Zhou, *et al.*, "A robust high refractive index sensitivity fiber Mach-Zehnder interferometer fabricated by femtosecond laser machining and chemical etching," *Sensors and Actuator A: Physical*, 2015, 230: 111–116.

[8] Z. Y. Li, C. R. Liao, Y. P. Wang, X. P. Dong, S. Liu, K. M. Yang, *et al.*, "Ultrasensitive refractive index sensor based on a Mach-Zehnder interferometer created in twin-core fiber," *Optics Letters*, 2014, 39(17): 4982–4985.

[9] Y. F. Zhang, C. P. Lin, C. R. Liao, K. M. Yang, Z. Y. Li, and Y. P. Wang, "Femtosecond laser-inscribed fiber interface Mach-Zehnder interferometer for temperature-insensitive refractive index measurement," *Optics Letters*, 2018, 43(18): 4421–4424.

[10] J. T. Zhou, C. R. Liao, Y. P. Wang, G. L. Yin, X. Y. Zhong, K. M. Yang, *et al.*, "Simultaneous measurement of strain and temperature by employing fiber Mach-Zehnder interferometer," *Optics Express*, 2014, 22(2): 1680–1686.

[11] M. S. A. Garcia, M. Bianchetti, R. L. Corre, A. Guevel, R. I. M. Chavez, J. M. S. Hernandez, *et al.*, "High sensitivity strain sensors based on single-mode-fiber core-offset Mach-Zehnder interferometers," *Optics and Lasers in Engineering*, 2018, 107: 202–206.

[12] L. C. Li, L. Xia, Z. H. Xie, L. N. Hao, B. B. Shuai, and D. M. Liu, "In-line fiber Mach-Zehnder

interferometer for simultaneous measurement of refractive index and temperature based on thinned fiber," *Sensors and Actuator A: Physical*, 2012, 180: 19–24.

[13] C. Y. Zhao, H. M. Qiu, H. J. Chen, X. H. Hu, Q. Q. Yu, Z. G. Lian, *et al.*, "In-fiber Mach-Zehnder temperature sensor using silicone-oil-filled dual core fiber," *Sensors and Actuator A: Physical*, 2021, 323: 112644–112649.

[14] S. C. Liu, Y. Huang, C. L. Deng, C. Y. Hu, C. H. Huang, Y. H. Dong, *et al.*, "Magneto-refractive properties and measurement of an erbium-doped fiber," *Optics Express*, 2021, 29(21): 34577–34589.

[15] Z. Y. Xiong, C. Y. Guan, Z. Y. Duan, T. L. Cheng, P. Ye, J. Yang, *et al.*, "All-optical vector magnetic field sensor based on a side-polished two-core fiber Michelson interferometer," *Optics Express*, 2022, 30(13): 22746–22754.

[16] M. M. Sun, Y. X. Jin, and X. Y. Dong, "All-fiber Mach-Zehnder interferometer for liquid level measurement," *IEEE Sensors Journal*, 2015, 15(7): 3984–3988.

[17] T. Jiao, H. Y. Meng, S. Y. Deng, S. Liu, X. J. Wang, Z. C. Wei, *et al.*, "Simultaneous measurement of refractive index and temperature using a Mach-Zehnder interferometer with forward core-cladding-core recoupling," *Optics & Laser Technology*, 2019, 111: 612–615.

[18] S. Y. Wang, Y. W. Ma, W. H. Chen, S. J. Wang, Y. Yi, X. Y. Li, *et al.*, "Ultrasensitive strain sensor based on Mach-Zehnder Interferometer with bent structures," *Journal of Lightwave Technology*, 2021, 39(21): 6958–6967.

[19] T. Q. Liu, J. Wang, Y. P. Liao, X. Wang, and S. S. Wang, "All fiber Mach-Zehnder interferometer for tunable two quasi-continuous points' temperature sensing in seawater," *Optics Express*, 2018, 26: 12277–12290.

[20] F. J. Harris, "On the use of windows for harmonic analysis with the discrete Fourier transform," *Proceedings of the IEEE*, 1978, 66(1): 51–83.

[21] I. Kanatov, D. Kaplun, D. Butusov, V. Gulvanskii, and A. Sinitca, "One technique to enhance the resolution of discrete Fourier transform," *Electronics*, 2019, 8(3): 330.

[22] S. Kumar, K. Singh, and R. Saxena, "Analysis of Dirichlet and generalized 'Hamming' window functions in the fractional Fourier transform domains," *Signal Processing*, 2011, 91(3): 600–606.

[23] L. J. Li, Q. Ma, M. Y. Cao, S. S. Gong, W. X. Li, X. Z. Ding, *et al.*, "Simulation and analysis of sensing modes of in-fiber interferometer," *Acta Poysica Sinica*, 2017, 6(22): 130–136.

[24] Y. Cao, H. Y. Liu, Z. R. Tong, S. Yuan, and J. Su, "Simultaneous measurement of temperature and refractive index based on Mach-Zehnder interferometer cascaded with a fiber Bragg grating," *Optics Communications*, 2015, 342(1): 180–183.

[25] W. J. Zhang, X. Q. Wu, G. Zhang, J. H. Shi, C. Zuo, S. S. Fang, *et al.*, "Simultaneous measurement of refractive index and temperature or temperature and axial strain based on an inline Mach-Zehnder interferometer with TCF-TF-TCF structure," *Applied Optics*, 2021, 50(6): 1522–1528.